Measurement of $K^*\bar{K}^*$ production in two-photon interactions

The ARGUS Collaboration

H. Albrecht, T. Hamacher, R. P. Hofmann, T. Kirchhoff, R. Mankel[a], A. Nau, S. Nowak[b], D. Reßing,
H. Schröder, H. D. Schulz, M. Walter[b], R. Wurth
DESY, Hamburg, Germany

C. Hast, H. Kapitza, H. Kolanoski[a] A. Kosche, A. Lange, A. Lindner, M. Schieber, T. Siegmund, H. Thurn, D.
Töpfer, D. Wegener
Institut für Physik[c], Universität Dortmund, Germany

C. Frankl, J. Graf, M. Schmidtler, M. Schramm, K. R. Schubert, R. Schwierz, B. Spaan, R. Waldi
Institut für Kern- und Teilchenphysik[d], Technische Universität Dresden, Germany

K. Reim, H. Wegener
Physikalisches Institut[e], Universität Erlangen-Nürnberg, Germany

R. Eckmann, H. Kuipers, O. Mai, R. Mundt, T. Oest, R. Reiner, A. Rohde, W. Schmidt-Parzefall
II. Institut für Experimentalphysik, Universität Hamburg, Germany

J. Stiewe, S. Werner
Institut für Hochenergiephysik[f], Universität Heidelberg, Germany

K. Ehret, W. Hofmann, A. Hüpper, K. T. Knöpfle, J. Spengler
Max-Planck-Institut für Kernphysik, Heidelberg, Germany

P. Krieger[g], D. B. MacFarlane[h], J. D. Prentice[g], P. R. B. Saull[h], K. Tzamariudaki[h], R. G. Van de Water[g], T.-S.
Yoon[g]
Institute of Particle Physics[i], Canada

M. Schneider, S. Weseler
Institut für Experimentelle Kernphysik[j], Universität Karlsruhe, Germany

M. Bračko, G. Kernel, B. Kerševan, P. Križan, E. Križnič, G. Medin[k], T. Podobnik, T. Živko
Institut J. Stefan and Oddelek za fiziko[l], Univerza v Ljubljani, Ljubljana, Slovenia.

V. Balagura, S. Barsuk, I. Belyaev, R. Chistov, M. Danilov, V. Eiges, L. Gershtein, Yu. Gershtein, A. Golutvin, O.
Igonkina, I. Korolko, G. Kostina, D. Litvintsev, P. Pakhlov, S. Semenov, A. Snizhko, I. Tichomirov, Yu. Zaitsev
Institute of Theoretical and Experimental Physics[m], Moscow, Russia

Abstract. A measurement of gamma–gamma production of the final states $K^+K^-\pi^+\pi^-$, $K^+K^-\pi^0\pi^0$, $K^0_S K^0_S \pi^+\pi^-$, $K^0_S K^\pm \pi^\mp \pi^0$ and $K^0_S K^0_S \pi^0\pi^0$ was performed by the ARGUS collaboration at the e^+e^- storage ring DORIS II at DESY. Since the two intermediate states $K^{*0}\bar{K}^{*0}$ and $K^{*+}K^{*-}$ are accessible by analysing different final states, the measurement provides several cross checks for cross-sections to these two states. The results for $\gamma\gamma \to K^*\bar{K}^*$ cross-sections obtained from different final states are found to be consistent with each other. The analysis of the partial wave structure of the $K^{*0}\bar{K}^{*0}$ state from the reaction $\gamma\gamma \to K^+K^-\pi^+\pi^-$ revealed the dominance of the $(J^P, J_z) = (2^+, \pm 2)$ wave.

1 Introduction

Over the last two decades, the two-photon production of vector meson pairs has been measured for all possible combinations of the mesons ρ, ω, ϕ and K^* in the energy region a few GeV above the thresholds [1–7]. The only exception is the combination $\phi\phi$ that has a, so far undetectable, small cross-section.

The interest in two-photon production of vector meson pairs was prompted by the observation of a large resonance-like cross-section for the reaction $\gamma\gamma \to \rho^0\rho^0$ in the invariant mass region near the nominal $\rho^0\rho^0$ threshold [1,4]. The attention was further enhanced by the measurement of the cross-section of the isospin related reaction $\gamma\gamma \to \rho^+\rho^-$ which was found to be at least four times smaller. Attempts have been made to explain these results by resonant [8–10] or non-resonant [11–13] mechanisms. The former imply an interference between an isospin $I = 0$ state and an exotic (e.g. $qq\bar{q}\bar{q}$) isospin $I = 2$ resonance.

It appears though that no single model can explain all the measured cross-sections. A systematic study of the accessible vector meson pair production channels is important for further progress in this field. A peculiarity of the reaction $\gamma\gamma \to K^*\bar{K}^*$ is that the vector mesons cannot be produced diffractively without the exchange of quarks.

The production of a pair of K^* mesons was first reported by ARGUS [5,6]. The analysis presented in this paper involved the complete ARGUS sample of events, which means the use of about twice as much data as in the previous analyses. The main purpose of this work was to extract cross-sections for the two–photon production of $K^{*0}\bar{K}^{*0}$ and $K^{*+}K^{*-}$, and to determine their spin-parity structure where possible. The reaction $\gamma\gamma \to K^*\bar{K}^*$ can be reconstructed in several final states as listed in Table 1. A powerful consistency check is provided by studying the production of the same $K^*\bar{K}^*$ intermediate state through different final state particles.

2 Selection of data

The two-photon production of the final states $K^+K^-\pi^+\pi^-$, $K^0_S K^\pm \pi^\mp \pi^0$, $K^0_S K^0_S \pi^+\pi^-$, $K^0_S K^0_S \pi^0\pi^0$ and $K^+K^-\pi^0\pi^0$ was observed in the reactions:

Table 1. The $K^{*0}\bar{K}^{*0}$ and $K^{*+}K^{*-}$ decay channels considered in the presented analysis. Particular branching ratios are determined by the fraction of K^0_S in K^0 and $\bar{K}^0$, and by the isospin Clebsch–Gordan coefficients connecting $K^*\bar{K}^*$ states with their decay products. The quoted values were used to normalise $\gamma\gamma \to K^*\bar{K}^*$ cross-sections extracted from different final states

Vector-meson pair	Decay channel		Branching ratio
$K^{*0}\bar{K}^{*0}$	$K^+\pi^-$	$K^-\pi^+$	$\frac{4}{9}$
	$K^0_S\pi^0$	$K^-\pi^+$	$\frac{1}{2} \cdot \frac{2}{9}$
	$K^+\pi^-$	$K^0_S\pi^0$	$\frac{1}{2} \cdot \frac{2}{9}$
	$K^0_S\pi^0$	$K^0_S\pi^0$	$\frac{1}{4} \cdot \frac{1}{9}$
$K^{*+}K^{*-}$	$K^+\pi^0$	$K^-\pi^0$	$\frac{1}{9}$
	$K^0_S\pi^+$	$K^-\pi^0$	$\frac{1}{2} \cdot \frac{2}{9}$
	$K^+\pi^0$	$K^0_S\pi^0$	$\frac{1}{2} \cdot \frac{2}{9}$
	$K^0_S\pi^+$	$K^0_S\pi^-$	$\frac{1}{4} \cdot \frac{4}{9}$

$$e^+e^- \to e^+e^- K^+K^-\pi^+\pi^- \qquad (1)$$

$$e^+e^- \to e^+e^- K^0_S K^\pm \pi^\mp \pi^0 \qquad (2)$$

$$e^+e^- \to e^+e^- K^0_S K^0_S \pi^+\pi^- \qquad (3)$$

$$e^+e^- \to e^+e^- K^0_S K^0_S \pi^0\pi^0 \qquad (4)$$

$$e^+e^- \to e^+e^- K^+K^-\pi^0\pi^0. \qquad (5)$$

The analysis presented in this paper was performed using data collected with the ARGUS detector at the e^+e^- storage ring DORIS II at DESY. The data correspond to an integrated luminosity of 456 pb^{-1} collected at beam energies between 4.7 GeV and 5.3 GeV. The ARGUS detector, its trigger and its particle identification system are described elsewhere [14]. In what follows, the main features of the analyses are presented (some details can be found in [15]).

The final state electrons scatter predominantly close to the beam direction and escape detection. Events selected for the above reactions had to satisfy the following conditions. Candidates for reactions (1), (2) and (4) were selected from events with four charged tracks and zero net charge in the final state. For reaction (3) candidate events consisted of six charged tracks with zero net charge, while only two oppositely charged tracks were required for reaction (5). Candidate tracks for charged pions and kaons had to be consistent with the corresponding mass hypothesis by requiring the ratio of the combined likelihood from specific ionisation and time-of-flight measurements to exceed 1%. In the case of reactions (1) and (5), all charged particles had to originate from a main vertex close to the nominal interaction point. For reactions (2) and (3) we required at least two oppositely charged tracks from a main vertex, while the remaining charged tracks had to originate from a K^0_S. In order to increase the efficiency, separate secondary vertices for K^0_S mesons were not required. Two oppositely charged particles associated with a K^0_S candidate had to
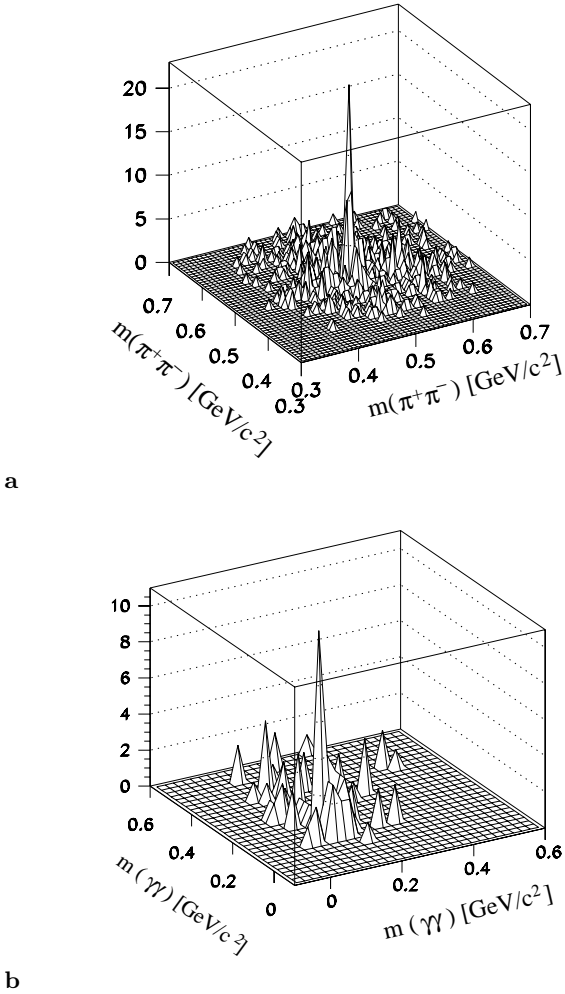
a

b

Fig. 1. a Invariant mass of a $\pi^+\pi^-$ associated with one K_S^0 versus the invariant mass of a $\pi^+\pi^-$ pair associated with the remaining K_S^0 for the $K_S^0 K_S^0 \pi^+\pi^-$ data. **b** Invariant mass of two photons versus the invariant mass of the remaining photons for the reaction $\gamma\gamma \to K_S^0 K_S^0 \pi^0\pi^0$

be identified as pions with likelihoods exceeding 1%. For illustration, Fig. 1a shows the invariant mass of a $\pi^+\pi^-$ pair associated with one K_S^0 versus the invariant mass of the remaining $\pi^+\pi^-$ pair associated with the second K_S^0 from the $K_S^0 K_S^0 \pi^+\pi^-$ selected sample. To be accepted as a K_S^0 candidate, the difference $|m(\pi^+\pi^-) - m(K_S^0)|$ between the invariant mass of the associated pion pair, $m(\pi\pi)$, and the nominal K_S^0 mass, $m(K_S^0)$, was required to be less than 12 MeV/c^2: according to the studies with simulated events this corresponds to 2.5 standard deviations of the $m(\pi\pi)$ resolution function.

Photons were identified by the energy deposited in clusters of modules of the electromagnetic calorimeter that were well separated from impact points of charged particles. The minimum energy required for photons ranged between 50 MeV and 110 MeV, depending on the noise level in the calorimeter modules. These levels were obtained from randomly recorded events where no photons are expected. For the candidates for reactions (2), (4) and (5), two detected photons were combined into a neutral pion if the invariant mass of the pair, $m(\gamma\gamma)$, was

close to the nominal π^0 mass $m(\pi^0)$: the maximum allowed mass difference, $|m(\gamma\gamma) - m(\pi^0)|$, was 70 MeV/$c^2$. The invariant mass of two photons versus the invariant mass of the remaining photon pair from the sample of preselected $\gamma\gamma \to K_S^0 K_S^0 \pi^0\pi^0$ candidates is presented in Fig. 1b. For the reactions (4) and (5) at least one $\pi^0\pi^0$ combination was required. In the case of more than one combination in the event, the combination with the smallest value of $\chi^2 = (m(\gamma\gamma) - m(\pi^0))^2 / \sigma^2(m(\gamma\gamma))$ was used, where $\sigma^2(m(\gamma\gamma))$ is the uncertainty on $m(\gamma\gamma)$ resulting from the measurement of photon energies. Monte Carlo studies showed that in this way more than 92% of π^0 mesons were correctly reconstructed. In order to improve the momentum resolution, π^0 candidates were subjected to 1-C fit to the π^0 nominal mass. Apart from the photons associated with the neutral pions, no other photons were allowed in the accepted events.

For all reactions, a cut on the total transverse momentum, $|\sum_i \overrightarrow{p}_{T,i}| < 100$ MeV/c, was applied to suppress the background.

Figure 2 shows distributions of invariant masses of one $K\pi$ combination with respect to the invariant masses of the remaining $K\pi$ combination in the same event for $K^+K^-\pi^+\pi^-$, $K_S^0 K^\pm \pi^\mp \pi^0$ and $K_S^0 K_S^0 \pi^+\pi^-$ candidates. The recoil $K\pi$ mass spectra are also presented in the same figure. To obtain the recoil mass spectra we required the invariant mass of one of the $K\pi$ combinations in an event to be between 0.8 GeV/c^2 and 1.0 GeV/c^2 and plotted the invariant mass, i.e. the recoil mass, of the remaining $\bar{K}\pi$ combination. Enhancements of events can be observed around the K^* nominal mass.

3 The method of data analysis

In general, a two-photon production of a certain set of final state particles f involves several intermediate states with different spins and parities - referred to as partial waves or hypotheses. Let us denote them by k. The number of events, $N^{(i)}(f)$, observed in the final state f and in a certain interval i of the two-photon invariant mass $W_{\gamma\gamma}$, is obtained as a sum over contributions of all possible partial waves k:

$$N^{(i)}(f) = L_{e^+e^-} \frac{d\mathcal{L}_{\gamma\gamma}^{(i)}}{dW_{\gamma\gamma}} \Delta W_{\gamma\gamma} \qquad (6)$$

$$\times \left(\sum_k \sigma^{(i)}(\gamma\gamma \to k) \cdot BR(k \to f) \cdot \eta^{(i)}(k \to f) \right),$$

where $L_{e^+e^-}$ is the time integrated luminosity, while $\frac{d\mathcal{L}_{\gamma\gamma}^{(i)}}{dW_{\gamma\gamma}}$ is the average two-photon luminosity function in the interval i and $\Delta W_{\gamma\gamma}$ is the width of the intervals. The average cross-section for the production of the partial wave k in the particular $W_{\gamma\gamma}$ interval is $\sigma^{(i)}(\gamma\gamma \to k)$, the branching ratio for the decay of the intermediate state k into the final state f is $BR(k \to f)$, and $\eta^{(i)}(k \to f)$ is the detector acceptance for that channel averaged over the full solid angle.
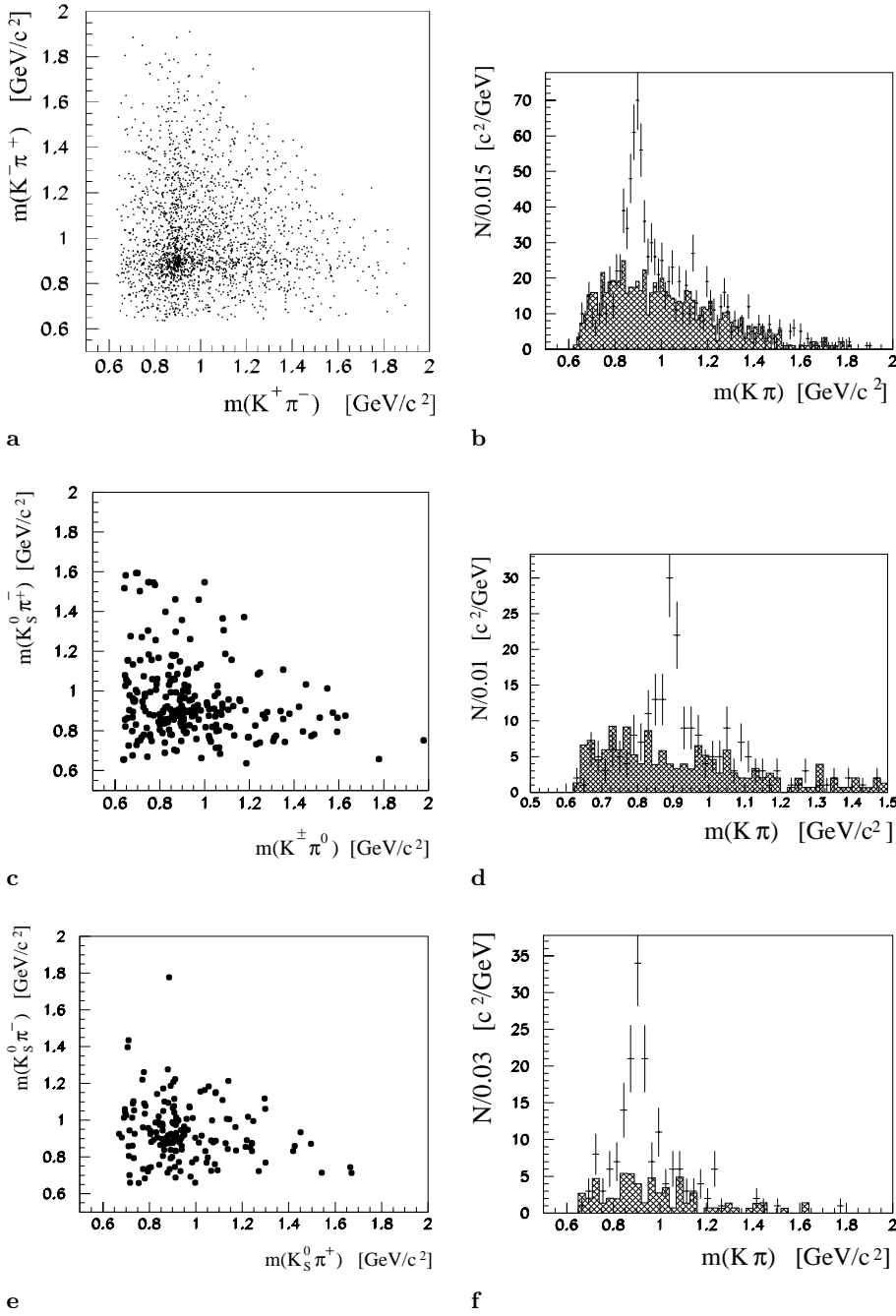
Fig. 2a–f. First column: invariant mass distributions of one $K\pi$ combination versus the distribution of the remaining $K\pi$ combinations for **a** $K^+K^-\pi^+\pi^-$, **c** $K^0_S K^\pm \pi^\mp \pi^0$ and **e** $K^0_S K^0_S \pi^+\pi^-$ (two entries per event) selected events. Second column: recoil mass spectra for **b** $K^\pm \pi^\mp$ (two entries per event), **d** $K^0_S \pi^\pm (K^\pm \pi^0)$ (two entries per event), and **f** $K^0_S \pi^\mp$ (four entries per event) candidates. The hatched histograms show the expected contributions from the background processes and from the nonresonant $2K2\pi$ production. The latter were normalised according to the previously measured cross-sections [5],[6]

The aim of the analysis was to determine the cross-sections $\sigma^{(i)}(\gamma\gamma \to k)$ for the partial waves k. They were obtained by requiring a maximum value of the likelihood function L. To obtain the likelihood function we proceeded in the following way: For each event j in the particular final state f, the set of measured quantities ξ_j (invariant masses and angles) was inserted in the probability density function, leaving fractions λ_k^2 of the measured events that were attributed to the particular partial waves as free parameters. The following expression [4] was maximised by varying the values of the fractions λ_k^2 for each $W_{\gamma\gamma}$ bin separately:

$$\ln L^{(i)} = \sum_{j=1}^{j=N^{(i)}(f)} \ln \left(\sum_k \frac{\lambda_k^{2(i)}}{\eta^{(i)}(k \to f)} \frac{|T_{k \to f}^{(i)}(\xi_j)|^2}{\overline{|T_{k \to f}^{(i)}|^2}} \right)$$
$$- N^{(i)}(f) \sum_k \lambda_k^{2(i)} . \tag{7}$$

Here $N^{(i)}(f)$ stands for the number of accepted events in a given final state f and $W_{\gamma\gamma}$ interval. $T_{k \to f}^{(i)}(\xi)$ represents the decay matrix element. Average squared matrix elements $\overline{|T_{k \to f}^{(i)}|^2}$ and average acceptances $\eta^{(i)}(k \to f)$ incor-

porated into the likelihood function were determined from Monte Carlo simulated data. Partial waves with the same naturality and helicity J_z can interfere with each other. Since the *a posteriori* result of the partial wave analysis that was performed in the $K^+K^-\pi^+\pi^-$ final state (see Sect. 4 and Table 2) showed that at least one of the amplitudes of the two states that could in principle interfere was always negligibly small, we restricted the likelihood function to non-interfering terms.

Final state particles were treated as a composition of two well defined isobars $K^*\bar{K}^*$ and isotropic contributions. It means that a uniform angular distribution was assumed for the $K^*K\pi$ and nonresonant $2K2\pi$ productions. On the other hand, the decay of a state with spin-parity J^P into two vector mesons is in general determined by different amplitudes, depending on the spin component J_z of the initial states, the orbital angular momentum L and the total spin S of the final state.

Gauge invariance and Bose symmetry forbid the states that would be formed by a fusion of two real photons and would have odd spin and negative parity, as well as those with spin 1 or $\gamma\gamma$-helicity 1. They also fix the $\gamma\gamma$-helicity of the states with even spin and negative parity to 0 and that of the states with odd spin and positive helicity to 2, while the states with even spin and positive parity can be produced in both $\gamma\gamma$-helicities [16].

The possible values of $K^*\bar{K}^*$ orbital angular momenta are $L = 1$ for $J^P = 0^-$, $L = 0, 2$ for $J^P = 0^+$, $L = 1, 3$ for $J^P = 2^-$, $L = 0, 2, 4$ for $J^P = 2^+$, and so on. The numbers of events in the selected samples were small: 1112 events for the $K^+K^-\pi^+\pi^-$ final state and even less for the other final states. Therefore the description of the data had to be further simplified in order to ensure the convergence of the likelihood function maximisation. Since the majority of the $\gamma\gamma \rightarrow K^*\bar{K}^*$ production was observed close to the kinematic threshold (see Sect. 4) we felt justified in restricting orbital angular momenta to $L = 0$ and $L = 1$. Thus, for the events with $K^+K^-\pi^+\pi^-$ in the final state, an analysis with 5 partial waves simultaneously associated to the $K^*\bar{K}^*$ was performed. For the other final states, the numbers of selected events were even smaller, so the $K^*\bar{K}^*$ production was described by a single partial wave at a time. Tests performed on different samples of simulated events showed that in this way only a negligible fraction of events, produced in the $K^*\bar{K}^*$ channel, was falsely ascribed to the isotropic channels. Due to the dominance of the wave with $(J^P, J_z) = (2^+, \pm 2)$ observed in the $K^+K^-\pi^+\pi^-$ final state (see Sect. 4) as well as in the production of vector meson pairs $\rho^0\rho^0$ and $\rho^+\rho^-$ [4], the cross-sections obtained with that particular wave are quoted as our final results (Tables 2, 3, 4, and 5). The difference between the quoted values and the values obtained by describing $K^*\bar{K}^*$ with other spins and parities, served as an estimate for the systematic uncertainties of the analysis (see Sect. 5 and Tables 6 and 7).

The main sources of background for all the final states considered were other two-photon interactions with incompletely reconstructed events or misidentified particles. To determine the numbers of background events attributed
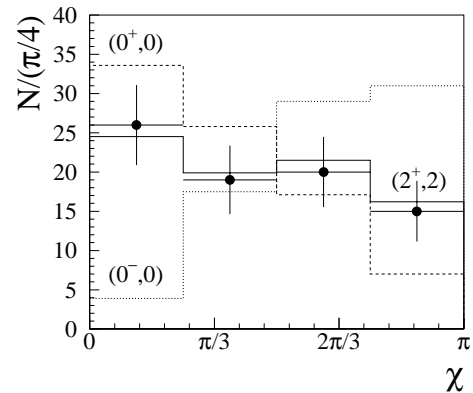

Fig. 3. Distributions of measured and simulated events with respect to the angle between the K^{*0} and the $\bar{K}^{*0}$ decay planes. Data (dots with error bars) are compared to the simulated distributions for $(2^+, 2)$ (full-line histogram), $(0^+, 0)$ (dashed histogram) and $(0^-, 0)$ (dotted histogram) $K^{*0}\bar{K}^{*0}$ partial waves

to a particular channel, an event generator based on measured $\gamma\gamma$ cross-sections [7,17] was used. Simulated samples were then subjected to the same selection criteria as the measured data. Consequently the partial wave analysis was repeated on the remaining background events. The fractions $\lambda^2_{k,bg}$ of the background events, attributed to particular partial waves k, were obtained from the results of the fit for a certain $W_{\gamma\gamma}$ interval i. For all final states and $W_{\gamma\gamma}$ intervals, the majority of the background was attributed to the isotropic channels.

Having determined $\lambda^{2(i)}_k$ and $\lambda^{2(i)}_{k,bg}$ inside a $W_{\gamma\gamma}$ interval i, the two-photon cross-section for the production of a certain partial wave $\sigma_{\gamma\gamma\rightarrow k}$ is given as follows:

$$\sigma^{(i)}_{\gamma\gamma\rightarrow k} = \frac{N^{(i)}(f)\lambda^{2(i)}_k - N^{(i)}_{bg}(f)\lambda^{2(i)}_{k,bg}}{L_{e^+e^-}\ \eta^{(i)}(k \rightarrow f)\ \frac{d\mathcal{L}^{(i)}_{\gamma\gamma}}{dW_{\gamma\gamma}}\Delta W_{\gamma\gamma}\ Br(k \rightarrow f)}\ .$$
(8)

In the above relation, $N^{(i)}_{bg}(f)$ is the number of expected background events for the particular final state f. The uncertainties on the background normalisation [7,17] were propagated to the uncertainties on the measured partial wave cross-sections and were included in the statistical errors on the quoted results.

4 Results of the analysis and discussion

$\underline{\gamma\gamma \rightarrow K^+\pi^- K^-\pi^+}$

After imposing the selection criteria, 1112 $K^+\pi^- K^-\pi^+$ events remained in the $W_{\gamma\gamma}$ region between 1.5 and 3.0 GeV/c^2. About 37% of these events were due to background contributions (mainly $\gamma\gamma \rightarrow \pi^+\pi^-\pi^+\pi^-$ events with pions misidentified as kaons).

The spin - parity analysis of $K^{*0}\bar{K}^{*0}$ was performed in three steps. The purpose of the first step was to obtain a rough estimate of various contributions to the $\gamma\gamma \rightarrow$

Table 2. Cross-sections (in nanobarns) for the processes $\gamma\gamma \to K^{*0}\bar{K}^{*0}$, $\gamma\gamma \to K^{*0}\bar{K}^-\pi^+$ + c.c., $\gamma\gamma \to \rho^0\phi$ and $\gamma\gamma \to K^+K^-\pi^+\pi^-$ as obtained by the three-step partial wave analysis of the $K^+K^-\pi^+\pi^-$ final state. The cross-sections for the intermediate states involving $K^{*0}\bar{K}^{*0}$ and $\rho^0\phi$ are normalised using the appropriate branching ratios (see Table 1) to the final state. When calculating the error of the sum of partial waves $\sum K^{*0}\bar{K}^{*0}$, the correlations of errors on cross sections for partial waves (J^P, J_z) were taken into account

	$W_{\gamma\gamma}$ [GeV/c^2]	$(0^+,0)$	$(2^-,0)$	$(2^+,\pm 2)$	$(2^+,0)$	$(0^-,0)$	$\sum K^{*0}\bar{K}^{*0}$	$K^{*0}K^-\pi^+$ + c.c.	$\rho^0\phi$	$K^+K^-\pi^+\pi^-$
1$^{\text{st}}$ step	1.75 - 2.25	0.58±1.10	0.77±0.59	3.26±1.30	-0.11±0.24	-0.06±0.62	4.44±1.25	5.10±0.70	1.42±1.19	3.80±0.30
2$^{\text{nd}}$ step	1.75 - 2.00	0.45±1.57	0.95±0.90	4.72±1.12	–	–	6.12±1.26	5.07±0.80	1.63±0.85	2.90±0.80
	2.00 - 2.25	0.90±1.80	0.27±1.57	3.06±0.70	–	–	4.23±1.90	6.60±1.32	1.22±0.76	4.10±1.20
	2.25 - 2.50	-0.45±0.90	0.65±1.50	0.81±0.70	–	–	1.01±1.30	4.43±0.80	0.65±0.33	3.00±1.10
3$^{\text{rd}}$ step	1.50 - 1.75	–	–	1.02±0.63	–	–	1.02±0.63	0.46±0.82	0.73±1.12	1.90± 0.65
	1.75 - 2.00	–	–	5.90±1.05	–	–	5.90±1.05	5.46±1.37	1.65±0.85	2.75±0.61
	2.00 - 2.25	–	–	3.75±0.90	–	–	3.75±0.90	7.09±1.13	1.21±0.76	4.02±0.92
	2.25 - 2.50	–	–	1.23±1.06	–	–	1.23±1.06	4.36±1.27	0.63±0.33	2.95±1.42
	2.50 - 2.75	–	–	0.46±0.90	–	–	0.46±0.90	4.75±1.28	-0.25±0.41	1.60±1.36
	2.75 - 3.00	–	–	0.40±0.72	–	–	0.40±0.72	3.58±0.64	0.27± 0.5	1.90±1.40

Table 3. Cross-sections (in nanobarns) for the processes $\gamma\gamma \to K^{*+}K^{*-}$, $\gamma\gamma \to K^{*0}\bar{K}^{*0}$, $\gamma\gamma \to K^{*+}K_S^0\pi^-$ + c.c., $K^+\pi^0 K^{*-}$ + c.c. and $K_S^0 K^+\pi^-\pi^0$ + c.c. obtained from the likelihood analysis of the $K_S^0 K^\pm \pi^\mp \pi^0$ final state

$W_{\gamma\gamma}$ [GeV/c^2]	$K^{*+}K^{*-}$	$K^{*0}\bar{K}^{*0}$	$K^{*+}K_S^0\pi^-$+ c.c.	$K^+\pi^0 K^{*-}$+ c.c.	$K_S^0 K^+\pi^-\pi^0$+ c.c.
1.75 - 2.00	28.80±5.98	5.63±2.95	-0.66±3.63	0.60±0.62	7.41±2.06
2.00 - 2.25	34.75±7.10	2.25±2.34	-0.72±3.00	-0.12±0.69	8.00±2.41
2.25 - 2.50	15.11±5.85	-0.78±3.11	8.40±5.70	1.89±1.8	7.42±2.11
2.50 - 2.75	3.20±2.97	0.25±3.45	5.40±3.90	0.64±1.51	3.88±1.63

$K^{*0}\bar{K}^{*0}$ cross-section. This was done with a partial wave analysis that included five $K^{*0}\bar{K}^{*0}$ waves with different spins and parities $|(L,S)J^P, J_z\rangle$: $|(0,0)0^+, 0\rangle$, $|(1,1)0^-, 0\rangle$, $|(0,2)2^+, \pm 2\rangle$, $|(0,2)2^+, 0\rangle$, $|(1,2)2^-, 0\rangle$, and three phase space distributed channels $K^{*0}K^-\pi^+$ + c.c., $K^+\pi^-K^-\pi^+$ and $\rho^0\phi$. The latter was included in the fit since a previous ARGUS analysis [7] determined that a sizeable fraction of the overall number of $\gamma\gamma \to K^+K^-\pi^+\pi^-$ events proceeded through the formation of the intermediate $\rho^0\phi$ state. The total intrinsic spin S of the system $K^{*0}\bar{K}^{*0}$ is the sum of the spins of both particles. The likelihood procedure was performed in a single bin with $W_{\gamma\gamma}$ between 1.75 and 2.25 GeV/c^2 that contains most of the data. The cross-section for the $J^P = 2^+$ wave was found to be dominant with the helicity 0 component suppressed if compared to the helicity 2 component, as already observed in the production of other tensor states in $\gamma\gamma$ reactions. The contributions from negative parities 0^- and 2^- were small. The results of the fit are in agreement with the expectations based on comparisons of measured angular distributions and the distributions simulated for different partial waves. As an example, Fig. 3 shows distributions of measured and simulated events with respect to the angle χ between the K^{*0} and the $\bar{K}^{*0}$ decay planes.

In the second step of the analysis, the $(J^P, J_z) = (2^+, 0)$ and the $J^P = 0^-$ $K^{*0}\bar{K}^{*0}$ channels, whose am-

plitudes were found in the first step of the analysis to be statistically not significantly different from zero, were excluded from the likelihood function (7). The reduced number of waves allowed for a division of the $W_{\gamma\gamma}$ range into 3 bins.

As a cross-check, the third step of the analysis was also performed by describing all $K^{*0}\bar{K}^{*0}$ channels by a single, i.e. $(2^+, \pm 2)$, wave. The analysis showed that about 14% of the total cross-section for $K^+K^-\pi^+\pi^-$ production is due to the formation of the $K^{*0}\bar{K}^{*0}$ intermediate state. The $\gamma\gamma \to K^{*0}\bar{K}^{*0}$ cross-sections obtained (see Fig. 4 and Table 2) agree within a few percent with the results of the second step of the analysis.

Note that our cross-sections are also comparable with the previously published ARGUS values [5] based on a smaller sample and analysed by the use of mass cuts. It is also interesting to compare the present result for the $\gamma\gamma \to \rho\phi$ cross-section (Fig. 4b) to that already published by ARGUS [7] and obtained by analysing the same event sample but again using a method based on mass cuts: the two results almost coincide.

$\gamma\gamma \to K_S^0 K^\pm \pi^\mp \pi^0$ and $\gamma\gamma \to K_S^0 K_S^0 \pi^+\pi^-$

The total number of selected $K_S^0 K^\pm \pi^\mp \pi^0$ events in the $W_{\gamma\gamma}$ region between 1.75 GeV/c^2 and 2.75 GeV/c^2 was
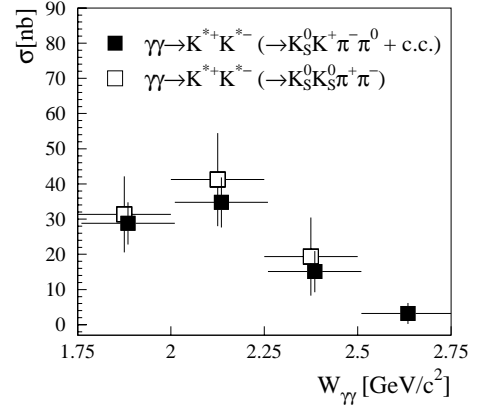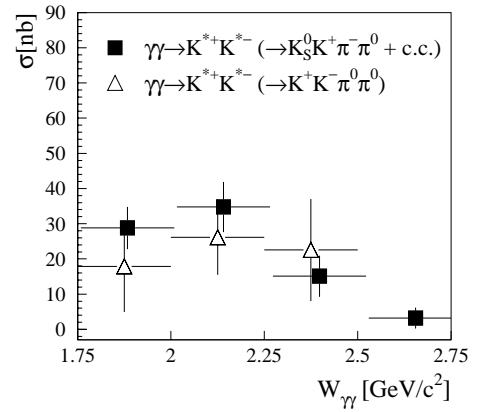
a

b
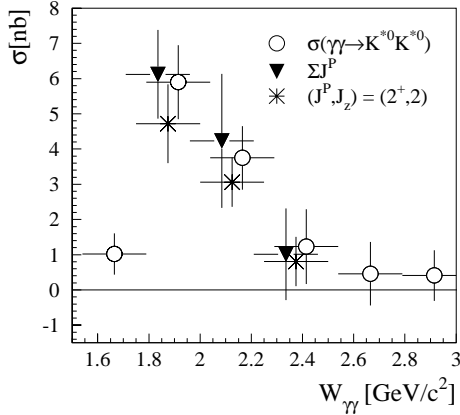
a
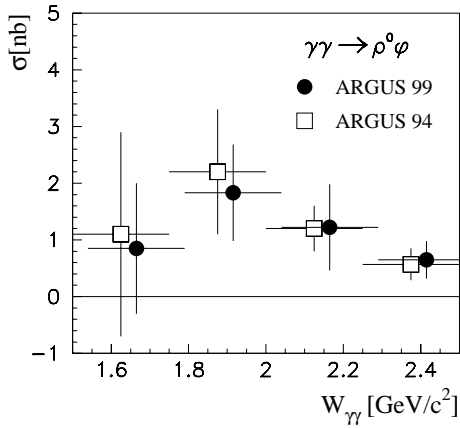
b

Fig. 4. a Cross-section for the sum of the $(J^P, J_z) = (0^+, 0)$, $(0^-, 0)$, $(2^+, 2)$ partial waves of the reaction $\gamma\gamma \to K^{*0}\bar{K}^{*0}$ (full triangles) and the cross-section for the dominant wave $(2^+, 2)$ (stars) from the second step of the $K^+K^-\pi^+\pi^-$ partial wave analysis. Open circles mark the $K^{*0}\bar{K}^{*0}$ cross-sections from the third step of the analysis (see text for a detailed description of different steps). **b** Comparison of the present results for the cross-section for the reaction $\gamma\gamma \to \rho^0\phi$ (full circles) to the results of the previous ARGUS analysis (open squares)[7]. Data points marked with symbols other than stars (**a**) and open squares (**b**) are slightly displaced in horizontal direction in order to make the comparison easier

Fig. 5. a Background subtracted cross-sections for the reaction $\gamma\gamma \to K^{*+}K^{*-}$ obtained by analysing $K_S^0 K^\pm \pi^\mp \pi^0$ data (full squares) and $K_S^0 K_S^0 \pi^+\pi^-$ data (open squares). **b** The cross-sections extracted from the $K_S^0 K^\pm \pi^\mp \pi^0$ (full squares) and the $K^+K^-\pi^0\pi^0$ (open triangles) final states. Data points marked with full squares (**a** and **b**) are slightly displaced in horizontal direction in order to make the comparison easier

245, 21% out of them were estimated to be from background contributions (mainly due to $\gamma\gamma \to 2\pi^+2\pi^-2\pi^0$ and $\gamma\gamma \to 2\pi^+2\pi^-\pi^0$ reactions). The partial wave analysis of the selected sample in the two–photon invariant mass region between 1.75 and 2.25 GeV/c^2 showed (see Table 3) that the cross-section for the $\gamma\gamma \to K^{*0}\bar{K}^{*0}$ production integrated over the entire range is for about eight times smaller than the integrated cross-section for the $\gamma\gamma \to K^{*+}K^{*-}$ formation. The systematic uncertainties on the quoted $K^{*+}K^{*-}$ and $K^{*0}\bar{K}^{*0}$ cross-sections due to the restriction of partial $K^*\bar{K}^*$ waves were estimated to be 8% and 10%, respectively.

The total number of selected $K_S^0 K_S^0 \pi^+\pi^-$ events in the mass region between 1.75 GeV/c^2 and 2.5 GeV/c^2 was 84. No background events were found to contribute to this

sample. The analysis of the $K_S^0 K_S^0 \pi^+\pi^-$ data covered 3 bins in the two-photon center-of-mass region between 1.75 GeV/c^2 and 2.5 GeV/c^2. As seen from Fig. 5a and Tables 3 and 4, the $\gamma\gamma \to K^{*+}K^{*-}$ cross-sections obtained by the analysis of the $K_S^0 K_S^0 \pi^+\pi^-$ final state almost coincide with those deduced from the $K_S^0 K^\pm \pi^\mp \pi^0$ sample. They are also in good agreement with the previous ARGUS results [6].

$\gamma\gamma \to K^+K^-\pi^0\pi^0$ and $\gamma\gamma \to K_S^0 K_S^0 \pi^0\pi^0$

After applying the selection criteria, 34 $K^+K^-\pi^0\pi^0$ and 23 $K_S^0 K_S^0 \pi^0\pi^0$ events were found in the two-photon center-of-mass region between 1.5 GeV/c^2 and 2.5 GeV/c^2; 12% and 26 % of them were expected to be the background contributions, respectively.

The $K^+K^-\pi^0\pi^0$ data were analysed in three $W_{\gamma\gamma}$ bins covering the invariant mass region between 1.75 GeV/c^2 and 2.50 GeV/c^2, while $K_S^0 K_S^0 \pi^0\pi^0$ events were divided into two 25 MeV/c^2 wide bins between 1.75 GeV/c^2 and

Table 4. Cross-sections (in nanobarns) for the reactions $\gamma\gamma \to K^{*+}K^{*-}$, $\gamma\gamma \to K^{*+}K_S^0\pi^-$ + c.c. and $\gamma\gamma \to K_S^0 K_S^0 \pi^+\pi^-$ obtained from the analysis of the $K_S^0 K_S^0 \pi^+\pi^-$ final state

$W_{\gamma\gamma}$ [GeV/c^2]	$K^{*+}K^{*-}$	$K^{*+}K_S^0\pi^-$ + c.c.	$K_S^0 K_S^0 \pi^+\pi^-$
1.75 - 2.00	31.32±10.80	-0.63±1.38	3.27±1.58
2.00 - 2.25	41.23±13.21	3.24±2.25	1.23±0.76
2.25 - 2.50	19.36±11.07	-0.60±1.86	2.64±1.32

Table 5. Cross-sections (in nanobarns) for the reactions $\gamma\gamma \to K^{*0}\bar{K}^{*0}$ and $\gamma\gamma \to K^{*+}K^{*-}$, measured in the final states $K_s^0 K_S^0 \pi^0\pi^0$ and $K^+K^-\pi^0\pi^0$, respectively, and normalised using the appropriate branching ratios (Table 1). Only statistical errors are shown

$W_{\gamma\gamma}$ (GeV/c^2)	$K^{*0}\bar{K}^{*0}$	$K^{*+}K^{*-}$
1.75 - 2.00	7.41 ± 5.90	17.87 ± 12.96
2.00 - 2.25	1.08 ± 2.1	26.16 ± 10.68
2.25 - 2.50	-	22.54 ± 14.47

2.25 GeV/c^2. As in previously described analyses, the two-photon production of $K^*\bar{K}^*$ was represented in the likelihood function (7) by a single, i.e. $(2^+, \pm 2)$, wave. The cross-sections for the reaction $\gamma\gamma \to K^*\bar{K}^*$ obtained from the two final states are given in Table 5. They are consistent with the more accurate results from other channels. As an example, Fig. 5b shows a comparison of the $\gamma\gamma \to K^{*+}\bar{K}^{*-}$ cross-sections resulting from the channels $\gamma\gamma \to K^+K^-\pi^0\pi^0$ and $\gamma\gamma \to K_S^0 K^\pm\pi^\mp\pi^0$.

5 Estimation of systematic uncertainties

The maximum likelihood method was extensively tested on Monte Carlo generated events. Samples of different (J^P, J_z) and isobar compositions were generated and analysed in the same way as the measured data. In all cases the input data were correctly reproduced. The largest systematic errors were expected to arise from the restrictions to the numbers of $K^*\bar{K}^*$ partial waves and from the uncertainties on the determination of detector acceptances for the particular waves.

To estimate the $\gamma\gamma \to K^*\bar{K}^*$ cross-section uncertainties arising from the omission of partial waves in the fit, the analyses were performed with different spin-parity hypotheses attributed to the $K^*\bar{K}^*$ channel. The results of the tests showed that the corresponding errors differed for different final states but never exceeded 11% (see Tables 6 and 7).

To see the influence of acceptance accuracies on the determined $\gamma\gamma \to K^{*0}\bar{K}^{*0}$ cross-sections the analyses were repeated with the acceptances for particular waves varied within the estimated uncertainties. In this way the cross-sections attributed to specific waves varied within 12%. On
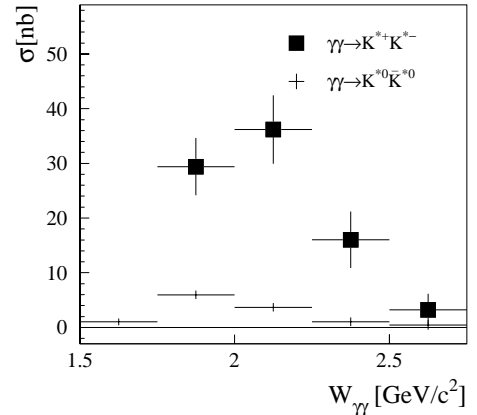

Fig. 6. Comparison of the cross-sections for the reactions $\gamma\gamma \to K^{*0}\bar{K}^{*0}$ (crosses) and $\gamma\gamma \to K^{*+}K^{*-}$ (squares). The $K^{*0}\bar{K}^{*0}$ cross-section is derived by combining $K^+K^-\pi^+\pi^-$ and $K_S^0 K^\pm\pi^\mp\pi^0$ analyses. The $K^{*+}K^{*-}$ cross-section is derived from $K_S^0 K^\pm\pi^\mp\pi^0$ and $K_S^0 K_S^0\pi^+\pi^-$ analyses

the other hand, since the determined partial wave cross-sections were mutually anti-correlated, the effect of such acceptance variations on the total $\gamma\gamma \to K^{*0}\bar{K}^{*0}$ cross-section was found to be small compared to the uncertainties due to the restrictions in the number of $K^*\bar{K}^*$ partial waves in the fit.

Other sources of systematic error are uncertainties on detector (6%) and trigger (5%) simulations and on luminosity measurements (1.8%), while the errors on the K^* branching ratios, $\text{BR}(K^* \to K\pi)$, are less than 0.2% [18] and thus negligible. Variations of event selection criteria, on the other hand, caused changes up to 5% in the extracted fractions λ_k^2.

A list of estimated systematic uncertainties on the $\gamma\gamma \to K^{*0}\bar{K}^{*0}$ and $\gamma\gamma \to K^{*+}K^{*-}$ cross-sections that were obtained from different final states are displayed in Tables 6 and 7.

6 Summary

The cross-sections for the reactions $\gamma\gamma \to K^{*0}\bar{K}^{*0}$ and $\gamma\gamma \to K^{*+}K^{*-}$ were obtained from the measurement of different final states. As a byproduct, the cross-section for the reaction $\gamma\gamma \to \rho^0\phi$ was also determined. It coincides with the one obtained by ARGUS using an independent analytical method. This provided an additional consistency check.

For the first time the final states $K^+K^-\pi^0\pi^0$ and $K_S^0 K_S^0\pi^0\pi^0$ were analysed. The extracted $\gamma\gamma \to K^*\bar{K}^*$ cross-sections from these analyses are consistent within statistical errors with the more accurate results from other channels.

The partial wave structure of the $K^{*0}\bar{K}^{*0}$ state was analysed using $K^+K^-\pi^+\pi^-$ data. It was found that the wave $(J^P, J_z) = (2^+, \pm 2)$ dominates.

The $\gamma\gamma \to K^{*0}\bar{K}^{*0}$ cross-section derived by combining the $K^+K^-\pi^+\pi^-$ and the $K_S^0 K^\pm\pi^\mp\pi^0$ analyses, and the $\gamma\gamma \to K^{*+}K^{*-}$ cross-section derived by combining the

Table 6. List of estimated systematic uncertainties on measured cross-section for the two-photon production of $K^{*0}\bar{K}^{*0}$

Final state	$K^+K^-\pi^+\pi^-$	$K_S^0\pi^0K^\pm\pi^\mp$	$K_S^0K_S^0\pi^0\pi^0$
Restriction of partial waves	7%	10%	11%
Variation of acceptance on J^P waves	2.3%	4.2%	8%
Selection criteria	1.6%	2.4%	4.8%
Detector simulation		6%	
Trigger simulation		5%	
Integrated luminosity		1.8%	
$\sum$	11%	14%	16.5%

Table 7. List of estimated systematic uncertainties on measured cross-section for the two-photon production of $K^{*+}K^{*-}$

Final state	$K_S^0K^\pm\pi^\mp\pi^0$	$K_S^0K_S^0\pi^+\pi^-$	$K^+K^-\pi^0\pi^0$
Restriction of partial waves	8%	5.6%	9.6%
Variation of acceptance on J^P waves	3.7%	3.9%	7.5%
Selection criteria	2.4%	3.6%	4.0%
Detector simulation		6%	
Trigger simulation		5%	
Integrated luminosity		1.8%	
$\sum$	12%	11%	15%

Table 8. Cross-sections (in nanobarns) for the reactions $\gamma\gamma \to K^{*0}\bar{K}^{*0}$ (derived by combining analyses of the final states $K^+\pi^-K^-\pi^+$ and $K_S^0\pi^0K^\pm\pi^\mp$) and $\gamma\gamma \to K^{*+}K^{*-}$ (derived by combining analyses of the final states $K_S^0\pi^0K^\pm\pi^\mp$ and $K_S^0K_S^0\pi^+\pi^-$). Only statistical errors are shown

$W_{\gamma\gamma}$ (GeV/c^2)	$\gamma\gamma \to K^{*0}\bar{K}^{*0}$	$\gamma\gamma \to K^{*+}K^{*-}$
1.50 - 1.75	1.02 ± 0.63	-
1.75 - 2.00	5.97 ± 0.78	29.40 ± 5.23
2.00 - 2.25	3.67 ± 0.77	36.20 ± 6.25
2.25 - 2.50	1.01 ± 0.79	16.04 ± 5.17
2.50 - 2.75	0.45 ± 0.87	3.20 ± 2.97

$K_S^0K^\pm\pi^\mp\pi^0$ and the $K_S^0K_S^0\pi^+\pi^-$ analyses, are displayed in Table 8 and Fig. 6. The results are in agreement with older ARGUS analyses [5,6] that involved only a part of the data. The ratio between the $\gamma\gamma \to K^{*+}K^{*-}$ and the $\gamma\gamma \to K^{*0}\bar{K}^{*0}$ cross-sections integrated in the mass region between 1.75 GeV/c^2 and 2.75 GeV/c^2 is $7.70 \pm 1.43 \pm 1.25$, where the first error is statistical and the second systematic.

The measured cross-sections allow for the various theoretical attempts to describe these gamma-gamma reactions to be tested. Various Regge exchange mechanisms [9] appear to be able to reproduce the two photon production of $K^{*0}\bar{K}^{*0}$ and $K^{*+}K^{*-}$ (including the $J^P = 2^+$ dominance). The perturbative QCD model of Brodsky et al. [12] does not account for the large values, but gives the correct ratios. Our measurements therefore constitute a continuing challenge to their proper theoretical description.

References

1. TASSO Collaboration, R. Brandelik et al., Phys. Lett. B **97** (1980) 448; Mark II Collaboration, D. L. Burke et al., Phys. Lett. B **103** (1981) 153; TASSO Collaboration, M. Althoff et al., Z. Phys. C **16** (1982) 13; CELLO Collaboration, H. J. Behrend et al., Z. Phys. C **21** (1984) 205; TPC/2γ Collaboration, H. Aihara et al., Phys. Rev. D **37** (1988) 28; PLUTO Collaboration, Ch. Berger et al., Z. Phys. C **38** (1988) 521

2. CELLO Collaboration, H.J. Behrend et al., Phys. Lett. B **218** (1989) 493; ARGUS Collaboration, H. Albrecht et al., Phys. Lett. B **267** (1991) 535

3. ARGUS Collaboration, H. Albrecht et al., Phys. Lett. B **196** (1987) 101; JADE Collaboration, A. Wegner et al., Z. Phys. C **48** (1990) 393; CELLO Collaboration, H. J. Behrend et al., Z. Phys. C **51** (1991) 365; ARGUS Collaboration, H. Albrecht et al., Phys. Lett. B **198** (1987) 577; ARGUS Collaboration, H. Albrecht et al., Phys. Lett. B **374** (1996) 265

4. ARGUS Collaboration, H. Albrecht et al., Z. Phys. C **50** (1991) 1

5. ARGUS Collaboration, H. Albrecht et al., Phys. Lett. B **198** (1987) 255

6. ARGUS Collaboration, H. Albrecht et al., Phys. Lett. B **212** (1988) 528

7. ARGUS Collaboration, H. Albrecht et al., Phys. Lett. B **332** (1994) 451

8. N. N. Achasov, S. A. Devyanin, G. N. Shestakov, Phys. Lett. B **108** (1982) 134; Z. Phys. C **16** (1982) 55, Z. Phys. C **27** (1985) 99

9. N. N. Achasov, V. A. Kornakov, G. N. Shestakov, Int. J. Mod. Phys. A **5** (1990) 2705

10. B. A. Li, K. F. Liu, Phys. Lett. B **118** (1982) 435 and Phys. Lett B **124** (1982) 550 (Erratum); Phys. Rev. Lett. **51** (1983) 1510; Phys. Rev. D **30** (1984) 613

11. G. Alexander, U. Maor, P. G. Williams, Phys. Rev. D **26** (1982) 1198; G. Alexander, A. Levy, U. Maor, Z. Phys. C **30** (1986) 65

12. S. J. Brodsky, G. Köpp, P. M. Zerwas, Phys. Rev. Lett. **58** (1987) 443

13. H. Kolanoski, Z. Phys. C **39** (1988) 543

14. ARGUS Collaboration, H. Albrecht et al., Nucl. Instr. Meth. A **275** (1989) 1

15. G. Medin, Measurement of Production of $K^{*0}\bar{K}^{*0}$ and $K^{*+}K^{*-}$ in Two-Photon Interactions at the ARGUS Spectrometer, Doctoral thesis, University of Ljubljana, Slovenia (1997)

16. L. D. Landau, Sov. Phys. Docl. **60** (1948) 207; C. N. Yang, Phys. Rev. **77** (1950) 242

17. T. Živko, Measurement of Production of $\rho^0\rho^0$, $\rho^+\rho^-$ and $\omega\omega$ in Two-photon Interactions at the ARGUS Spectrometer, Doctoral thesis, University of Ljubljana, Slovenia (1994); E. Križnič, Production of $\omega\rho^0$, $\rho^0\phi$ and $\omega\phi$ in Two-Photon Interactions at the ARGUS Spectrometer, Doctoral thesis, University of Ljubljana, Slovenia (1994); ARGUS Collaboration, H. Albrecht et al., Phys. Lett. B **210** (1988) 273; ARGUS Collaboration, H. Albrecht et al., Phys. Lett. B **212** (1988) 528

18. Particle Data Group, Review of Particle Physics, Eur. Phys. J. C **3** (1998) 1